Some researchers have pointed out that the cyclic motion of the arm is effective for controlling both arm shape and body orientation.[2–4] Our result verifies this property of a space robot when the mobility ranges of the joint angles are limited.

Experiments

The same experiment as Ref. 1 was performed. Because the path planned by the GA was the same as the breadth-first search in Ref. 1, the result is not described here.

In the case of optimal control, because the experiment is limited to a total time of 10 s, the path obtained using Eqs. (3–5) should be compressed to about 5.5 s. Moreover, because this robot cannot control the joint angles and angular velocities continuously, 20 discrete points from the path were used to execute the experiment. The results of joint motion are shown in Fig. 3a. The dotted lines indicate ideal compressed paths, and solid lines indicate the actual motions. They are in good agreement. In Fig. 3, the origin of time is taken as the time of initial robot motion. Figure 3b shows the camera images of the grid graph paper before and after the motion. The light source positions, represented by black circles, are slightly different, even though they should be the same. In Fig. 3c, (p_{1e}, p_{2e}) indicates the experimental results for the motion of the light source position effect on the image, and (p_{1s}, p_{2s}) represents the simulated results: p_2 motions are in good agreement, whereas p_1 motions are not.

There are four possible causes of error. The first is model inaccuracy. The second is error of the database itself. These have been explained previously.[3] However, the third and fourth possibilities are peculiar causes related to optimal control. The third possibility is the assumption of $\mathrm{d}p_i = \dot{p}_i$. Here $\mathrm{d}p_i$ was measured by moving the joints ±30 deg/s for 1 s, whereas $\dot{p}_i$ is the velocity of the image motion in a pixel, where infinitesimally small motion during an infinitesimally small time period is assumed. Obviously, the assumption of $\mathrm{d}p_i = \dot{p}_i$ is in error. The fourth possibility is motion beyond the database. The joint angle q_1 moves in the negative range during the motion, which is out of the database range. This might result in an error.

Conclusions

Based on the results, the following general conclusions can be made.

1) The merit of GA lies in finding a temporary path at an early stage.

2) The merit of using optimal control techniques lies in the ability to deal with continuous joint angle values.

3) Results verify the property of cyclic motion of the arm for control when the ranges of joint angles are limited.

Acknowledgments

This work is supported by the New Energy and Industrial Technology Development Organization through the Japan Space Utilization Promotion Center in the program of the Ministry of International Trade and Industry.

References

[1]Iwata, T., Kodama, K., Numajiri, F., and Murakami, H., "Experiments on Space Robot Arm Path Planning Using the Sensors Database," *Journal of Guidance, Control, and Dynamics*, Vol. 22, No. 4, 1999, pp. 573–578.

[2]Longman, R. W., "The Kinematics and Workspace of a Satellite-Mounted Robot," *Journal of Astronautical Sciences*, Vol. 38, No. 4, 1990, pp. 423–440.

[3]Nakamura, Y., and Suzuki, T., "Planning Spiral Motions of Nonholonomic Free-Flying Space Robots," *Journal of Spacecraft and Rockets*, Vol. 34, No. 1, 1997, pp. 137–143.

[4]Yamada, K., and Yoshikawa, S., "Feedback Control of Space Robot Attitude by Cyclic Arm Motion," *Journal of Guidance, Control, and Dynamics*, Vol. 20, No. 4, 1997, pp. 715–720.

[5]Wu, A. K., and Miele, A., "Sequential Conjugate Gradient-Restoration Algorithm for Optimal Control Problems with Non-Differential Constraints and General Boundary Conditions, Part I," *Optimal Control Applications and Methods*, Vol. 1, No. 1, 1980, pp. 69–88.

[6]Gonzalez, S., and Rodrigues, S., "Modified Quasilinearization Algorithm for Optimal Control Problems with Nondifferential Constraints and General Boundary Conditions," *Journal of Optimization Theory and Applications*, Vol. 50, No. 1, 1986, pp. 109–128.

Multiple Model-Based Terminal Guidance Law

Ilan Rusnak*
RAFAEL, Ministry of Defense, 31021 Haifa, Israel

I. Introduction

THERE are continuing efforts to improve the performance of guidance laws for the terminal phase of a missile intercepting maneuvering targets. More detailed models have been introduced for derivation of guidance laws with improved performance with respect to the classical proportional navigation. The inclusion of the stochastic nature of the measurements led to the introduction of Kalman filters into guidance.[1,2] The inclusion of the missile dynamics and target maneuver, by the use of the optimal control theory, was considered in Refs. 1, 3, and 4. When the target acceleration is unknown the shaping filter was used in Ref. 1 to account for the target's maneuver. The missile acceleration constraint has been dealt with in Ref. 3. The differential games approach has been presented in Refs. 5–7.

Here we concentrate on more detailed modeling of the target maneuver. Namely, the contribution of this paper is the application of the multiple model-based approach to the derivation of a guidance law for the terminal phase of a missile intercepting a maneuvering target. We consider the multiple model adaptive control (MMAC) architecture[8,9] and the multiple model adaptive estimation (MMAE)-based control architecture.[10] These architectures are suboptimal, feasible algorithms for control of uncertain systems. They have been applied to control of uncertain systems with success.[11]

The main objective is to assess the improvement in performance that can be achieved by application of the multiple model-based algorithm to the derivation of the guidance law: the multiple model-based guidance law (MMGL). The comparison between the guidance law based on the shaping filter[1] and the MMGL is performed on a common basis. By common basis we mean that the information available for both approaches is identical.

The guidance law based on the shaping filter is linear and time-varying. The MMGL is time-varying and nonlinear. A simple example is presented to identify the improvement and to keep the numerical effort affordable, as it increases rapidly with the number of model hypotheses. In the example we assume a missile with an instantaneous time response autopilot, guided against a maneuvering target that performs a step maneuver whose initiation instant is uniformly distributed over the short terminal intercept period. The simulations show that the MMGL has improved performance, in term of a smaller miss distance, with respect to the guidance law based on the shaping filter approach.

II. Statement of the Problem

The following is the problem of control on an nth-order stochastic linear discrete-time uncertain system on finite time.[8] The system is specified by the following model:

$$x(i+1) = A(\theta)x(i) + m(\theta, i) + b(\theta)u(i) + v(i), \qquad x(0) = x_0$$

$$y(i) = c(\theta)x(i) + w(i), \qquad i = 0, 1, 2, \ldots, N-1 \quad (1)$$

where $x(i) \in R^n$ is the state; $u(i) \in R^1$ is the input and $y(i) \in R^1$ is the measured output; $A(\theta) \in R^{n \times n}$ and $b(\theta)$, $c(\theta)^T \in R^n$; and $m(\theta, i) \in R^n$ is an external deterministic input for a given θ. The sequences $v(i)$ and $w(i) \in R^1$ are mutually independent excitation and observation noise processes, respectively. They are zero-mean white Gaussian sequences with covariances $E[v(i)v(j)^T] = V(j, \theta)\delta_{ij}$ and $E[w(i)w(j)^T] = W(j, \theta)\delta_{ij}$. The initial state vector x_0 is Gaussian and independent of $v(i)$ and $w(i)$ for $i \geq 0$ and has a priori probability density $p[x(0)]$ with mean $\bar{x}_0$ and covariance Q_0.

Received 5 May 1999; revision received 27 December 1999; accepted for publication 31 December 1999.

*Senior Research Scientist, P.O. Box 2250. Member AIAA.

The p-dimensional time-invariant parameter vector θ is unknown, with assumed a priori probability density function $p(\theta)$ defined on a fixed set Ω_θ.

Our interest is to derive a guidance law, i.e., to derive a sequence $\{u(0), u(1), u(2), \ldots, u(N-1)\}$, such that the cost function

$$J = \frac{1}{2}E\left[x(N)^T G x(N) + \sum_{i=0}^{N-1} u(i)^T u(i)\right] \tag{2}$$

is minimized subject to Eq. (1), where $0 \leq G \in R^{n\times n}$ and $0 < R \in R^1$. We are looking for an implementable control scheme, such that $u(i)$ is a function of the observations $\lambda_k = \{y(0), y(1), \ldots, y(k)\}$.

III. Multiple Model Control Algorithms

For the case of completely known systems, i.e., when the parameter vector is completely known, $p(\theta) = \delta(\theta - \theta_0)$, the solution of the above problem is well known.[2] It is a cascade of the Kalman filter and a full-state feedback. Certainty equivalence and separation apply in this case.

The solution of the problem defined in Sec. II is not feasible.[8] Therefore approximate schemes have been derived:

1) the MMAC[8,9] and

2) the MMAE-based control.[10]

These approaches assume that the range of the uncertain parameters θ is discrete or that it is suitably quantized, that is, $\Omega_\theta = \{\theta_1, \theta_2, \ldots, \theta_M\}$, where M is the number of elements in the uncertainty set.

A. MMAC

In the MMAC approach, the system state estimation is performed by the appropriate algorithm.[8] A block diagram of this algorithm is presented in Fig. 1. Specifically, the optimal state estimator for the jth hypothesis, $j = 1, 2, \ldots, M$, is given by

$$\begin{aligned}
\hat{x}_j(i+1\,|\,i) &= A(\theta_j)\hat{x}_j(i\,|\,i) + m(\theta_j, i) + b(\theta_j)u(i)\\
\hat{x}_j(0\,|\,0) &= \bar{x}_0\\
\nu_j(i+1) &= y(i+1) - c(\theta_j)\hat{x}_j(i+1\,|\,i)\\
\hat{x}_j(i+1\,|\,i+1) &= \hat{x}_j(i+1\,|\,i) + K_j(i+1)\nu_j(i+1)\\
i &= 1, 2, \ldots, N-1\\
Q_j(i+1\,|\,i) &= A(\theta_j)Q_j(i\,|\,i)A^T(\theta_j) + V(i, \theta_j)\\
Q_j(0\,|\,0) &= Q_0\\
S_j(i+1) &= c^T(\theta_j)Q_j(i\,|\,i)c(\theta_j) + W(i, \theta_j)\\
K_j(i+1) &= Q_j(i\,|\,i)c^T(\theta_j)S_j^{-1}(i+1)\\
K_j(i+1\,|\,i+1) &= Q_j(i+1\,|\,i) - K_j(i+1)S_j(i+1)K_j^T(i+1)
\end{aligned} \tag{3}$$

Under the Gaussian assumption the probability density function of the innovations is

$$p[\nu_j(i)] = [2\pi S_j(i)]^{-\frac{1}{2}} \exp\left[-\tfrac{1}{2}\nu_j^T(i)S_j(i)\nu_j(i)\right] \tag{4}$$

The posterior probability that the jth hypothesis is correct is

$$\pi_j(i) = \frac{p[\nu_j(i)]\pi_j(i-1)}{\sum_{j=1}^{M} p[\nu_j(i)]\pi_j(i-1)}, \qquad \pi_j(0) = \text{Prob}(\theta = \theta_j) \tag{5}$$

where $\pi_j(0)$, $j = 1, 2, \ldots, M$, is the a priori probability that the jth model is correct. The control is

$$u(i) = \sum_{j=1}^{M} u_j(i)\pi_j(i) = \sum_{j=1}^{M} F_j(i)\hat{x}_j(i\,|\,i)\pi_j(i), \qquad \sum_{j=1}^{M}\pi_j(i) = 1 \tag{6}$$

where $F_j(i)$ is a control law design for a known model with parameters θ_j. Here we assume that this control law is precomputed off-line by the Riccati equation as follows:

$$\begin{aligned}
u_j(i) &= F_j(i)\hat{x}_j(i\,|\,i)\\
F_j(i) &= -R^{-1}b(\theta_j)^T P_j(i+1)\left[I + b(\theta_j)^T R^{-1} b(\theta_j)^T\right.\\
&\quad \left.\times P_j(i+1)\right]^{-1} A(\theta_j), \qquad i = N-1, N-2, \ldots, 1, 0\\
P_j(i) &= A(\theta_j)^T P_j(i+1)\left[I + b(\theta_j)^T R^{-1} b(\theta_j)^T\right.\\
&\quad \left.\times P_j(i+1)\right]^{-1} A(\theta_j), \qquad P_j(N) = G
\end{aligned} \tag{7}$$

B. MMAE-Based Control

In the MMAE-based control approach, the system state estimation is performed by the estimation algorithm [Eq. (3)]. A block diagram of this algorithm is presented in Fig. 2. The estimated state is

$$\hat{x}(i+1\,|\,i+1) = \sum_{j=1}^{M} \hat{x}_j(i+1\,|\,i+1)\pi_j(i) \tag{8}$$

and the control is

$$u(i) = F[\hat{\theta}(i)]\hat{x}(i\,|\,i) \tag{9}$$

where the estimated parameters are

$$\hat{\theta}(i) = \sum_{j=1}^{M} \theta_j \pi_j(i) \tag{10}$$

and $F(\theta)$ is a control design rule yet to be specified (it is not specified here). There are no known proofs of stability or results on performance of the MMAC or MMAE-based control algorithms.

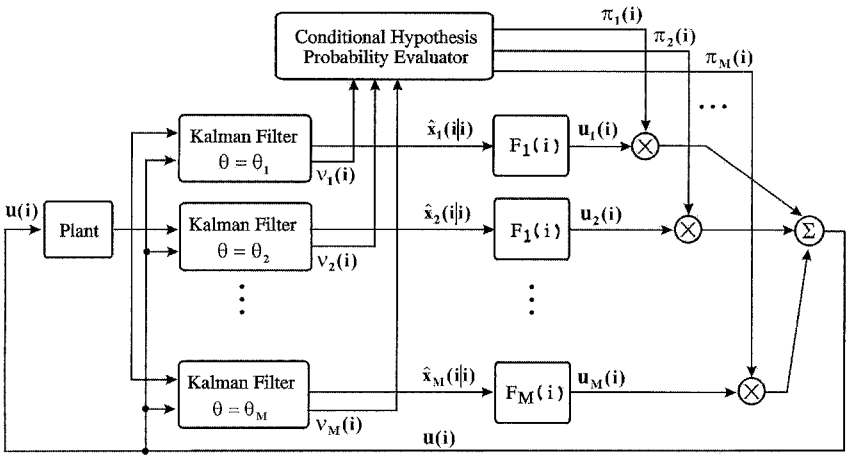

Fig. 1 Block diagram of the MMAC approach.

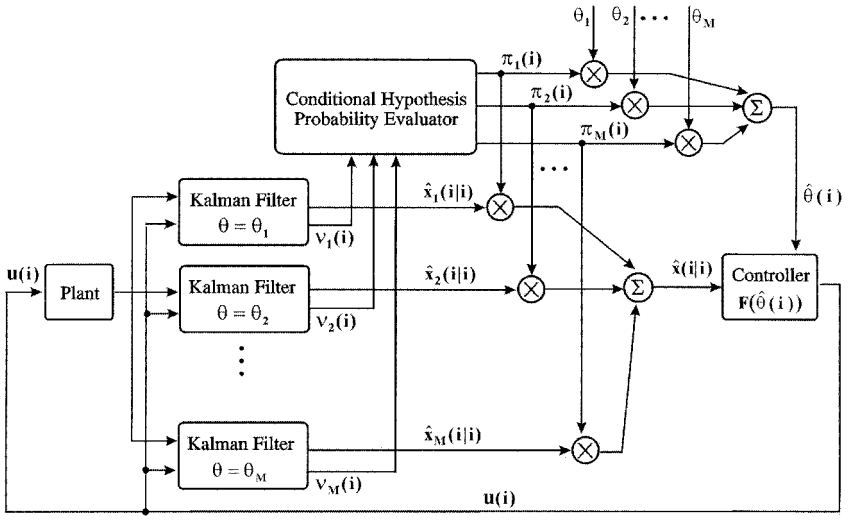

Fig. 2 Block diagram of the MMAE-based control approach.

IV. Derivation of a Guidance Law

To derive a guidance law we assume, similarly to Ref. 2 (p. 154), the following continuous system:

$$\frac{\mathrm{d}}{\mathrm{d}t}\begin{pmatrix}x(t)\\ \dot{x}(t)\end{pmatrix}=\begin{pmatrix}0 & 1\\ 0 & 0\end{pmatrix}\begin{pmatrix}x(t)\\ \dot{x}(t)\end{pmatrix}+\begin{pmatrix}0\\ 1\end{pmatrix}\xi a_{T0}\mu(t-\tau)-\begin{pmatrix}0\\ 1\end{pmatrix}u(t)$$

$$y(t)=[1\quad 0]\begin{pmatrix}x(t)\\ \dot{x}(t)\end{pmatrix}+w(t) \tag{11}$$

where $\mu(t)$ is the step function. This is a model of a target that initiates a step acceleration of amplitude a_{T0} at time $t=\tau$. The acceleration can be either positive or negative, i.e., ξ is a random variable such that $\xi\in\{-1, 1\}$, and $\text{Prob}(\xi=+1)=0.5$, $\text{Prob}(\xi=-1)=0.5$. The initiation instant, τ, is a random variable uniformly distributed in the interval $[0, t_f]$, $t_f=NT$, where T is the sampling interval. Thus the target's acceleration is a stochastic process, as the initiation instant and its direction are random variables.

To derive the MMGL we discretize the uncertainty set. That is, we approximate the uncertainty set $\{\tau\,|\,0\le\tau\le t_f\}\oplus\{\xi\,|\,\xi\in\{-1, 1\}\}$ by the finite set

$$\Omega_\theta=\{\tau_j=jT\,|\,j=0, 1, 2, \ldots, N-1\}\oplus\{\xi\,|\,\xi\in\{-1, 1\}\} \tag{12}$$

and

$$\pi_j(0)=\text{Prob}(\tau_k=\tau_j)=1/M \tag{13}$$

We have $M=2N$ hypotheses. The discrete system for the hypothesis that a target maneuver starts at instant kT is

$$\begin{bmatrix}x(i+1)\\ \dot{x}(i+1)\\ a_T(i+1)\end{bmatrix}=\begin{bmatrix}1 & T & \frac{1}{2}T^2\\ 0 & 1 & T\\ 0 & 0 & 1\end{bmatrix}\begin{bmatrix}x(i)\\ \dot{x}(i)\\ a_T(i)\end{bmatrix}-\begin{bmatrix}\frac{1}{2}T^2\\ T\\ 0\end{bmatrix}u(i)$$

$$+\begin{bmatrix}\frac{1}{6}T^3\\ \frac{1}{2}T^2\\ T\end{bmatrix}\frac{1}{T}[\xi_a a_{T0}\delta_{ik}+v(i)]$$

$$y(i)=[1\quad 0\quad 0]\begin{bmatrix}x(i)\\ \dot{x}(i)\\ a_T(i)\end{bmatrix}+w(i),\qquad i=0, 1, 2, \ldots, N-1 \tag{14}$$

where $\xi_a=+1$ for a positive maneuver and $\xi_a=-1$ for a negative maneuver.

In practice the actual maneuver initiates at τ_{mnv}, where $\tau_{mnv}\neq kT$, thus $v(i)$ represents the residual between the actual target acceleration and the assumed acceleration in the model.

The discrete Kalman filter for each hypothesis (3), $j=1, 2, \ldots, M$ $(M=2N)$, is

$$\begin{bmatrix}\hat{x}_j(i+1\,|\,i)\\ \hat{\dot{x}}_j(i+1\,|\,i)\\ \hat{a}_{Tj}(i+1\,|\,i)\end{bmatrix}=\begin{bmatrix}1 & T & \frac{1}{2}T^2\\ 0 & 1 & T\\ 0 & 0 & 1\end{bmatrix}\begin{bmatrix}\hat{x}_j(i\,|\,i)\\ \hat{\dot{x}}_j(i\,|\,i)\\ \hat{a}_{Tj}(i\,|\,i)\end{bmatrix}-\begin{bmatrix}\frac{1}{2}T^2\\ T\\ 0\end{bmatrix}u(i)$$

$$+\begin{bmatrix}\frac{1}{6}T^3\\ \frac{1}{2}T^2\\ T\end{bmatrix}\frac{1}{T}\xi_h a_{T0}\delta_{ik}$$

$$\nu_j(i+1)=y(i+1)-\hat{x}_j(i+1\,|\,i)$$

$$\begin{bmatrix}\hat{x}_j(i+1\,|\,i+1)\\ \hat{\dot{x}}_j(i+1\,|\,i+1)\\ \hat{a}_{Tj}(i+1\,|\,i+1)\end{bmatrix}=\begin{bmatrix}\hat{x}_j(i+1\,|\,i)\\ \hat{\dot{x}}_j(i+1\,|\,i)\\ \hat{a}_{Tj}(i+1\,|\,i)\end{bmatrix}+K_j(i+1)\nu_j(i+1)$$

$$i=0, 1, 2, \ldots, N-1 \tag{15}$$

where

$$k=\begin{cases}j-1 & \text{if}\quad 1\le j\le N\\ j-N-1 & \text{if}\quad N+1\le j\le 2N\end{cases}$$

$$\xi_h=\begin{cases}1 & \text{if}\quad 1\le j\le N\\ -1 & \text{if}\quad N+1\le j\le 2N\end{cases}$$

and the gain $K_j(\,)$ is as detailed in Eq. (3).

The discrete guidance law for each hypothesis, $j=1, 2, \ldots, M$ $(M=2N)$, is independent of the hypothesis for the presented special case and is derived based on the system

$$\begin{bmatrix}x(i+1)\\ \dot{x}(i+1)\\ a_T(i+1)\end{bmatrix}=\begin{bmatrix}1 & T & \frac{1}{2}T^2\\ 0 & 1 & T\\ 0 & 0 & 1\end{bmatrix}\begin{bmatrix}x(i)\\ \dot{x}(i)\\ a_T(i)\end{bmatrix}-\begin{bmatrix}\frac{1}{2}T^2\\ T\\ 0\end{bmatrix}u(i) \tag{16}$$

The guidance law is the augmented proportional navigation, which is presented for the continuous case in Ref. 1 (Chap. 7). The derivation for discrete systems is presented in the Appendix. The commanded acceleration for each hypothesis, for $G=[g\ \ 0\ \ 0]$, $R=1$, $g\to\infty$, is

$$u_j(i)=\frac{6(N-1)}{2(N-i)+1}$$

$$\times\frac{\hat{x}_j(i\,|\,i)+(N-i)T\hat{\dot{x}}_j(i\,|\,i)+\frac{1}{2}(N-i)^2T^2\hat{a}_{Tj}(i\,|\,i)}{(N-i)^2T^2} \tag{17}$$

and the commanded acceleration of the missile is

$$u(i) = \sum_{j=1}^{M} u_j(i)\pi_j(i) \tag{18}$$

where

$$\pi_j(0) = \text{Prob}(\tau_k = \tau_j)\text{Prob}(\xi = \xi_h) = 1/2N \tag{19}$$

Note that for the special case presented here we have

$$u(i) = \frac{6(N-i)}{2(N-i)+1} \times \frac{\hat{x}(i\,|\,i) + (N-i)T\hat{\dot{x}}(i\,|\,i) + \frac{1}{2}(N-i)^2T^2\hat{a}_T(i\,|\,i)}{(N-i)^2T^2} \tag{20}$$

where

$$\hat{x}(i\,|\,i) = \sum_{j=1}^{M} \hat{x}_j(i\,|\,i)\pi_j(i), \qquad \hat{\dot{x}}(i\,|\,i) = \sum_{j=1}^{M} \hat{\dot{x}}_j(i\,|\,i)\pi_j(i)$$

$$\hat{a}_T(i\,|\,i) = \sum_{j=1}^{M} \hat{a}_{Tj}(i\,|\,i)\pi_j(i) \tag{21}$$

Note that this is a special case of the MMAC-based control where the controller is independent of the hypothesis.

V. Shaping Filter-Based Guidance Law

The existing approach in deriving a guidance law[1] is to represent the target's acceleration by a shaping filter (Ref. 1, Chap. 4). Then the continuous system under consideration is (Ref. 1, Chap. 8)

$$\frac{\mathrm{d}}{\mathrm{d}t}\begin{bmatrix} x(t) \\ \dot{x}(t) \\ a_{T0}(t) \end{bmatrix} = \begin{bmatrix} 0 & 1 & 0 \\ 0 & 0 & 1 \\ 0 & 0 & 0 \end{bmatrix}\begin{bmatrix} x(t) \\ \dot{x}(t) \\ a_{T0}(t) \end{bmatrix} - \begin{bmatrix} 0 \\ 1 \\ 0 \end{bmatrix}u(t) + \begin{bmatrix} 0 \\ 0 \\ 1 \end{bmatrix}v_c(t)$$

$$y(t) = \begin{bmatrix} 1 & 0 & 0 \end{bmatrix}\begin{bmatrix} x(t) \\ \dot{x}(t) \\ a_{T0}(t) \end{bmatrix} + w_c(t) \tag{22}$$

where $E[v_c(t)v_c^T(t)] = V_c\delta(t-\tau)$, $V_c = a_{T0}^2/t_f$, and $E[w_c(t)w_c^T(t)] = W_c\delta(t-\tau)$.

The discrete system is

$$\begin{bmatrix} x(i+1) \\ \dot{x}(i+1) \\ a_T(i+1) \end{bmatrix} = \begin{bmatrix} 1 & T & \frac{1}{2}T^2 \\ 0 & 1 & T \\ 0 & 0 & 1 \end{bmatrix}\begin{bmatrix} x(i) \\ \dot{x}(i) \\ a_T(i) \end{bmatrix} - \begin{bmatrix} \frac{1}{2}T^2 \\ T \\ 0 \end{bmatrix}u(i) + \begin{bmatrix} \frac{1}{6}T^3 \\ \frac{1}{2}T^2 \\ T \end{bmatrix}\frac{1}{T}v(i)$$

$$y(i) = \begin{bmatrix} 1 & 0 & 0 \end{bmatrix}\begin{bmatrix} x(i) \\ \dot{x}(i) \\ a_T(i) \end{bmatrix} + w(i), \qquad i = 0, 1, 2, \ldots, N-1 \tag{23}$$

The Kalman filter for this system is presented in Ref. 1 (Chap. 9).

The discrete guidance law for the shaping filter is based on Eq. (16), and we have

$$u(i) = \frac{6(N-i)}{2(N-i)+1} \times \frac{\hat{x}(i) + (N-i)T\hat{\dot{x}}(i) + \frac{1}{2}(N-i)^2T^2\hat{a}_T(i)}{(N-i)^2T^2} \tag{24}$$

VI. Simulations Results

Here we present simulation results of comparison between the guidance law based on the shaping filter approach, detailed in Sec. V, and the guidance law based on the multiple model-based approach, detailed in Sec. IV. The example is kept simple to identify the improvement and to keep the numerical effort affordable. Namely, we assume that the target acceleration level is known. In practice its value, and not only its direction, should be included in the uncertainty set. Such inclusion would have increased the numeric effort to an unacceptable level. The evaluation is performed by the Monte Carlo method. The results are presented for 1000 runs, $T = 0.1$ s, and $W_c = 1\ \text{m}^2/\text{Hz}$. For the MMGL $V_c = 1\ \text{m}^2/\text{s}^5$, and for the shaping filter guidance law $V_c = a_{T0}^2/t_f$, and $a_{T0} = 50\ \text{m/s}^2$. The simulation initiates when the missile is on the collision course, i.e., $x(0) = 0$ and $\dot{x}(0) = 0$.

Table 1 RMS miss of the multiple model-based and shaping filter-based guidance laws

	RMS miss, m, at t_f				
	1 s	2 s	3 s	4 s	5 s
Shaping filter	3.34	3.14	2.89	2.81	2.75
MMGL	2.63	2.18	1.92	1.85	1.7

The mean of the miss is zero, as the direction of the target's maneuver is positive or negative with equal probability. The RMS miss for the two types of guidance laws at several terminal times is presented in Table 1. We can see that the MMGL is a vital approach for deriving a guidance law for the final phase of a homing missile. As can be seen the MMGL has a smaller RMS miss distance. This improvement is due solely to the more detailed modeling of the target's maneuver and the additional computational effort.

VII. Conclusions

A guidance law based on the multiple model approach has been derived. Simulations show that, at the expense of large numerical effort, the MMGL is capable of improving missile performance with respect to the shaping filter-based guidance law.

Appendix: (Title)

In Ref. 4 the discrete guidance law for high-order missile and maneuvering target was derived. In the example considered here we assume a zero-lag autopilot and a step target maneuver, i.e.,

$$\frac{a_m(z)}{u(z)} = 1, \qquad \frac{a_m(z)}{a_m(0)} = \frac{z}{z-1}, \qquad \frac{a_T(z)}{a_T(0)} = \frac{z}{z-1} \tag{A1}$$

then as $g \to \infty$, the effective navigation ratio, $N'(i)$, is

$$N'(i) = (N-i)^2T^2\Lambda(N-i) = \frac{6(N-i)}{[2(N-i)+1]} \tag{A2}$$

and not the erroneous result in Eq. (14) in Ref. 4. The guidance law is the augmented proportional navigation,

$$u(i) = N'(i)\frac{x(i) + (N-i)T\dot{x}(i) + \frac{1}{2}(N-i)^2T^2a_T(i)}{(N-i)^2T^2} = N'(i)\left(V_{\text{close}}\dot{\lambda}(i) + \frac{1}{2}a_T(i)\right) \tag{A3}$$

where $\dot{\lambda}(i)$ is the inertial line-of-sight angular rate, and V_{close} is the closing velocity.

References

[1]Zarchan, P., *Tactical and Strategic Missile Guidance*, 3rd ed., Vol. 176, Progress in Astronautics and Aeronautics, AIAA, Washington, DC, 1997.

[2]Bryson, A. E., and Ho, Y. C., *Applied Optimal Control*, Hemisphere, New York, 1975, Chap. 5.

[3]Rusnak, I., and Levi, M., "Optimal Guidance for High-Order and Acceleration Constrained Missile," *Journal of Guidance, Control, and Dynamics*, Vol. 14, No. 3, 1991, pp. 589–596.

[4]Rusnak, I., "Discrete Optimal Guidance for High-Order Missile and Maneuvering Target," *IEEE Transactions on Aerospace and Electronic Systems*, Vol. 27, No. 6, Nov. 1991, pp. 870–872.

[5]Forte, I., and Shinar, J., "Can a Mixed Guidance Strategy Improve Missile Performance?" *Journal of Guidance, Control, and Dynamics*, Vol. 11, No. 1, 1988, pp. 53–59.

[6]Forte, I., and Shinar, J., "Improved Guidance Law Design Based on the Mixed-Strategy Concept," *Journal of Guidance, Control, and Dynamics*, Vol. 12, No. 5, 1989, pp. 739–745.

[7]Ben-Asher, J., and Yaesh, I., *Advances in Missile Guidance Theory*, Vol. 180, Progress in Astronautics and Aeronautics, AIAA, Washington, DC, 1998, Chap. 5.

[8]Deshpande, J. G., Upadhay, T. N., and Lainiotis, D. G., "Adaptive Control of Linear Stochastic Systems," *Automatica*, Vol. 9, 1973, pp. 107–115.

[9]Maybeck, P. S., *Stochastic Models, Estimation and Control*, Vol. 3, Academic, New York, 1984, pp. 247–257.

[10]Stepaniak, M. J., and Maybeck, P. S., "MMAE-Based Control Redistribution Applied to the VISTA F-16," *IEEE Transactions on Aerospace and Electronic Systems*, Vol. 34, No. 4, 1998, pp. 1249–1260.

[11]Maybeck, P. S., and Stevens, R. D., "Reconfigurable Flight Control via Multiple Model Adaptive Control Methods," *IEEE Transactions on Aerospace and Electronic Systems*, Vol. 27, No. 4, May 1991, pp. 470–480.

Class of Rotations Induced by Spherical Polygons

Ranjan Mukherjee* and Jay T. Pukrushpan†
Michigan State University,
East Lansing, Michigan 48824-1226

Introduction

THE geometry of rotations is critical to the analysis of diverse problems ranging from the motion of celestial bodies to the dexterous manipulation of objects subject to nonholonomic constraints. In a number of these problems, the use of orientation coordinates such as Euler angles[1] and Euler parameters[1] becomes necessary since angular velocities are nonintegrable in nature.[2] Though angular velocities fail to provide a proper choice of orientation coordinates, their nonintegrable nature provides greater control authority. It has been shown in recent years, for example, that complete reconfiguration of a rolling sphere in five dimensions is possible using only two angular velocities as control inputs.[3–5]

From our own research[5] on reconfiguration of the rolling sphere, it becomes clear that a certain sequence of rotations about axes confined to the horizontal plane is equivalent to a single rotation about the vertical axis. For the sequences proposed,[5] the point of contact between the sphere and the ground traces spherical triangles.[6,7] Though these results were obtained for a rolling sphere, they apply to general rigid body rotation. Also, closed curves on the sphere need not be restricted to spherical triangles; they can be lunes[8] or other spherical polygons.‡

The primary contribution of this Note lies in the use of spherical trigonometry for establishing a fundamental relationship in rotational kinematics, stated also by the Gauss–Bonet theorem[9] of parallel transport. The theorem essentially states that a rolling sphere, which depicts the rotational motion of a rigid body constrained to rotate about axes that are confined to one plane, undergoes a net change in orientation about the axis perpendicular to the plane when its point of contact traces a spherical polygon. The amount of rotation is equal to the solid angle enclosed by the polygon and the direction of rotation depends on the direction in which the polygon is traced. This result and its mathematical exposition reinforce the connection between spherical trigonometry and rotational kinematics, which has been pointed out in earlier works.[10] Apart from rotational kinematics, the result is also useful for other applications. For example, it helps us to us resolve the problem of image registration with space telescopes when they are pointed from one direction sequentially to other directions and back to the original direction, to generate an image of an extended region. The axis of the telescope traces out the edges of a spherical polygon on the infinite sphere when it is returned to its original pointing direction. To avoid the problem of image registration, one has to compensate for rotation of the telescope about its own axis, equal to the solid angle subtended by the traced spherical polygon.

Received 12 July 1999; revision received 15 October 1999; accepted for publication 17 January 2000.

*Associate Professor, Department of Mechanical Engineering. 2555 Engineering Building; mukherji@egr.msu.edu.

†Graduate Student.

‡In the spirit of the common terminology "spherical triangle," we define a "spherical polygon" as a closed curve on the surface of a sphere comprised of multiple segments wherein each segment is an arc of a great circle.

Review of Spherical Trigonometry

A circle generated by a plane passing through the center of a sphere is a great circle. The angle on the sphere formed by intersecting arcs of two great circles is a spherical angle. The portion of the sphere bounded by arcs of three great circles is called a spherical triangle. Consider the spherical triangle in Fig. 1, whose vertices and spherical angles are P, Q, R and A, B, C, respectively. Let a, b, c denote the angles subtended by the arcs QR, RP, PQ at the center of the sphere. The important relations for the spherical triangle[6–8] are given by the law of sines,

$$\sin a/\sin A = \sin b/\sin B = \sin c/\sin C \tag{1}$$

the laws of cosines for sides,

$$\cos a = \cos b\cos c + \sin b\sin c\cos A \tag{2}$$

$$\cos b = \cos c\cos a + \sin c\sin a\cos B \tag{3}$$

$$\cos c = \cos a\cos b + \sin a\sin b\cos C \tag{4}$$

and the laws of cosines for angles,

$$\cos A = -\cos B\cos C + \sin B\sin C\cos a \tag{5}$$

$$\cos B = -\cos C\cos A + \sin C\sin A\cos b \tag{6}$$

$$\cos C = -\cos A\cos B + \sin A\sin B\cos c \tag{7}$$

Some useful relationships that can be derived[6–8] from the laws of cosines for sides are

$$\sin A\cos b = \sin C\cos B + \sin B\cos C\cos a \tag{8}$$

$$\sin B\cos c = \sin A\cos C + \sin C\cos A\cos b \tag{9}$$

$$\sin C\cos a = \sin B\cos A + \sin A\cos B\cos c \tag{10}$$

$$\sin a\cos C = \sin b\cos c - \sin c\cos b\cos A \tag{11}$$

$$\sin b\cos A = \sin c\cos a - \sin a\cos c\cos B \tag{12}$$

$$\sin c\cos B = \sin a\cos b - \sin b\cos a\cos C \tag{13}$$

$$\sin A\cos c = \sin B\cos C + \sin C\cos B\cos a \tag{14}$$

$$\sin B\cos a = \sin C\cos A + \sin A\cos C\cos b \tag{15}$$

$$\sin C\cos b = \sin A\cos B + \sin B\cos A\cos c \tag{16}$$

The area of a spherical triangle can be mathematically expressed as

$$\Delta = Er^2, \qquad E \triangleq (A + B + C - \pi) \tag{17}$$

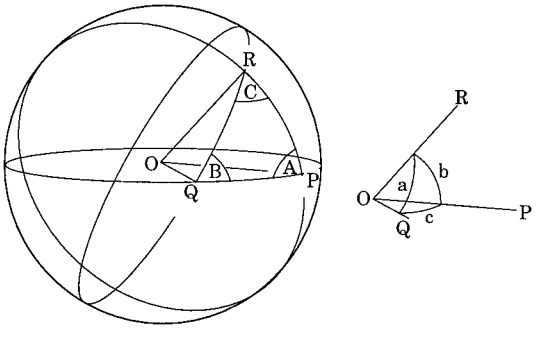

Fig. 1 Spherical triangle.